Biosensors and Bioelectronics 167 (2020) 112475

Contents lists available at ScienceDirect

Biosensors and Bioelectronics

journal homepage: http://www.elsevier.com/locate/bios

Ultrasensitive magnetic DNAzyme-copper nanoclusters fluorescent biosensor with triple amplification for the visual detection of *E. coli* O157:H7

Ziqi Zhou [a,b], Yangzi Zhang [a,b], Mingzhang Guo [a,b], Kunlun Huang [a,b], Wentao Xu [a,b,*]

[a] Key Laboratory of Precision Nutrition and Food Quality, Department of Nutrition and Health, China Agricultural University, Beijing, 100083, China
[b] Key Laboratory of Safety Assessment of Genetically Modified Organism (Food Safety) (MOA), College of Food Science and Nutritional Engineering, China Agricultural University, Beijing, 100083, China

ARTICLE INFO

Keywords:
E. coli O157:H7
DNAzyme
Fluorescent biosensor
RCA
Magnetic beads
Copper nanocluster

ABSTRACT

A relatively-simple and high-efficient fluorescent magnetic biosensor based on DNAzyme was established for the detection of *E. coli* O157:H7. In order to solve the problem of weak signal and low sensitivity in the detection of foodborne pathogenic bacteria, we ingeniously designed a fluorescent sensor based on triple signal amplification of magnetic beads, DNAzyme and photoluminescence. In the detection process, the *E. coli*-specific RNA-cleaving DNAzyme can specifically identify the target protein in crude intracellular mixture (CIM), which caused its conformation changes and induced rolling circle amplification (RCA) to the generation and luminescence of copper nanoclusters (CuNCs). This cascade amplification design can capture weak signals in the sample. The biosensor also indicated a good linear range from 10 CFU mL^{-1} to 1000 CFU mL^{-1} and obtained a limit of detection (LOD) of 1.57 CFU mL^{-1}, which showed a relatively high sensitivity compared with other studies. Furthermore, the biosensor displayed high-efficient detection capability in 1.5 h and good reproducibility (relative standard deviations < 2%). It has been proved that this sensor is feasible to the detection of *E. coli* O157:H7 in drinking water and apple juice. Moreover, we found that the final detection product can effectively wrap the magnetic beads and can be driven by the magnetic field. And this unexpected discovery will provide ideas for the development of biosensing robots.

1. Introduction

E. coli O157:H7 is the main pathogenic serotype of enterohemorrhagic *E. coli* (EHEC) with widespread routes and low infectious dose. This food-borne pathogen with healthy cattle or sheep as the host produces the shiga toxin transmitted by beef products, milk, contaminated water, and other routes (Saeedi et al., 2017). Patients infected with this type of *E. coli* are prone to cause diarrhea and hemorrhagic enteritis, and easily develop secondary hemolytic uremic and thrombotic thrombocytopenic purpura with a low infectious dose (Cooper et al., 2014; Saeedi et al., 2017). This type of *E. coli* poses still a serious threat to human health in areas of poor sanitation, imperfect medical security system, high-density population and complex demographic composition (Bedasa et al., 2018).

The infection prevalence of *E. coli* O157:H7 can be monitored and controlled by the advanced detection techniques to avoid us from severe infection (Guo et al., 2019). The detection strategies of *E. coli* O157:H7 are diverse and each of them has their superiorities and limitations. The traditional plate culture method (or called bacterial separation method) is a simple and cost-saving method for identifying and detecting pathogenic bacteria, but it can hardly achieve rapid detection because of its dependence on long culture cycle. Moreover, due to the mutation of the strain or the uneven distribution of selective substances it is prone to produce false negative or positive results, respectively (McConnell et al., 2020). In contrast, polymerase chain reaction (PCR) technology can achieve the quantitative detection in a relatively short period of time with a lower concentration of the target bacteria, but this relatively costly and complicated operation may present false positive or non-visual results, and cannot carry out the on-site detection in high-population areas (Tian et al., 2019). In addition, quantitative PCR

* Corresponding author. Key Laboratory of Precision Nutrition and Food Quality, Department of Nutrition and Health, China Agricultural University, No. 17, Qinghua East Road, Beijing, 100083, China.
E-mail address: xuwentao@cau.edu.cn (W. Xu).

https://doi.org/10.1016/j.bios.2020.112475
Received 26 May 2020; Received in revised form 21 July 2020; Accepted 22 July 2020
Available online 31 July 2020

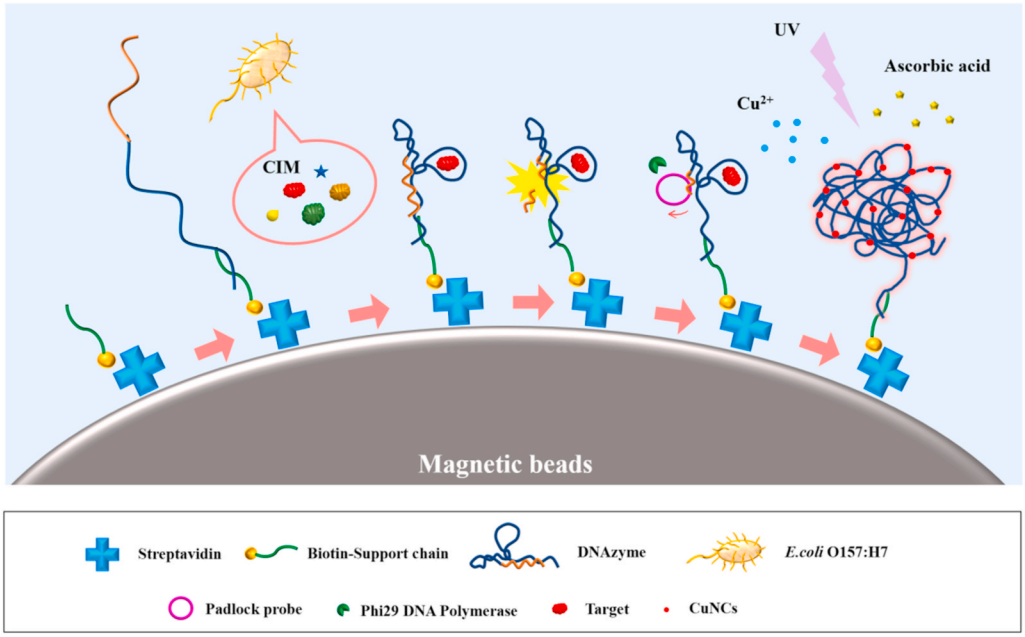

Scheme. 1. Magnetic DNAzyme-CuNCs fluorescent biosensor for the detection of *E. coli* O157:H7.

(qPCR) is the most commonly-used method for detecting pathogenic bacteria, but it cannot achieve constant temperature detection (Sluijter et al., 2006) and increases difficulty of detection on a certain extent. Similar problems from Raman spectroscopy and surface plasmon resonance have been reported (Cho et al., 2015; Wang et al., 2016). Furthermore, although antibody-related immunoassays can effectively capture the target bacteria in samples and reduce false positives (Xu et al., 2016), the high price and instability of antibodies also increase expenses of detection (Song et al., 2019a,b).

Functional nucleic acids (FNAs) is a type of nucleic acid with special functions (McConnell et al., 2020; Xiao et al., 2019; Xu et al., 2019). They have both a stable structure and the potential to form special functions based on higher-level conformations. Based on the affinity between them and targets, FNAs can be easily screened through the systematic evolution of ligands by exponential enrichment (SELEX) technique in vitro. Therefore, FNAs as inexpensive and high-efficient tools of target identification have been widely affirmed in a variety of biosensors for rapid detection (Li, 2011).

Deoxyribozymes, also called DNAzymes, are a class of FNAs which possess the integrated properties of aptamers and enzymes (Chen et al., 2016; Zhu et al., 2017), mainly including RNA cleaving activity, DNA ligase activity, DNA hydrolysis activity, DNA kinase activity, N2 glycosylase activity, and DNA cap activity, amongst other (Flynn-Charlebois et al., 2003; Vaish et al., 2003; Cho et al., 2005; Gong et al., 2015). Among various activities, DNAzyme with peroxidase-like activity and RNA cleaving activity is most used for detection. For example, Hemin-bound G-quadruplex, one of the peroxidase-like activity DNAzymes, can be cleverly used to amplify the photoelectric signal of the reaction (Lv et al., 2017b; Zhang et al., 2017). The other most commonly-used DNAzyme, RNA-cleaving DNAzyme is one type of 8–17 DNAzyme and was first discovered through mRNA processing. When the target material is present in the system, the RNA-cleaving DNAzyme can catalyze cleavage of the RNA specific sites, thereby breaking the mRNA and inducing its transcription implementation on the regulation of gene expression (Rothenbroker et al., 2019). It can cleave chimeric ribonucleotide sites in DNA sequences (Ma and Zhang, 2019), namely hydrolysis 3′ end dihydrogen phosphate ester bond of RNA to achieve chain rupture (Ali et al., 2012). And this DNAzyme have been used for detection of many targets, such as heavy metal ions and bacterial. (Zhou et al., 2016; Ali et al., 2011). *E. coli*-specific DNAzymes have been obtained by in vitro screening (Ali et al., 2011). Using this DNAzyme, Yu et al. (2017) built the magnetic bead-DNAzyme detection system and realized signal output by using localized surface plasmon resonance to improve the efficiency of detection. Subsequently, Yousefi et al. (2018) designed a covalent binding of the fluorescent DNAzyme cleaved by *E. coli*-specific RNA with transparent cyclic olefin copolymer (COP) film, thereby realizing the detection of microorganisms in plastic-sealed food. Additionally, Liu et al. (2016) developed a single-stranded topology detection method with improved sensitivity. Furthermore, the RNA-cleaving DNAzymes can be combined with other output strategies or equipment, such as litmus and paper sensors, to increase speed and portability of the on-site tests (Tram et al., 2014; Ali et al., 2017).

DNA-templated fluorescent metal nanoclusters can be perceived as another application of FNAs (Qing et al., 2017; Liu, 2014) for the reason that metal ions can bind to specific sites on bases and generate metal clusters in situ in the presence of reducing agents (Satyavolu et al., 2019). Compared with other metal nanoclusters, copper nanoclusters (CuNCs) not only have excellent fluorescence characteristics, but also have better biocompatibility and lower toxicity (Xia et al., 2019). More importantly, the size and their fluorescence intensity of CuNCs can be facilely controlled by adjusting the length of poly T. For example, fluorescent copper nanoparticles (CuNPs) can be obtained from the poly T-Cu^{2+} complex without any complicated modifications. These copper nanoclusters (CuNCs) can emit red light with a wavelength of 615 nm under excitation light with a wavelength of 340 nm (Qing et al., 2013). Thus, they are used as highly effective signal output tools for biosensors. A kind of FNA-generated-CuNCs has applied for the detection of alkaline phosphatase in serum (Yang et al., 2017). Using the different characteristics of copper ions and copper nanoclusters can superbly realize the change of the luminous state of the sensor device (Lv et al., 2017a).

In order to amplify the detection signal and improve the sensitivity of detection, we herein designed a novel thermostatic ultra-sensitive visual magnetic sensor to detect *E. coli* O157:H7 (Scheme 1). This sensor could achieve rapid and sensitive detection in a short time, which was based on triple signal amplification: (1) *E. coli*-specific DNAzyme (Ali et al., 2011; Aguirre et al., 2013) enriched target from complex environment depending on magnetic beads. (2) Targets induced the conformational changes of DNAzyme to trigger self-cutting of RNA site. The cutting fragments turned into the primer of RCA to finally obtain many repeated T-rich sequences. (3) In the reduced environment, CuNCs are rapidly

generated on these T-rich regions. Their fluorescence was excited at 340 nm and was turned all the chemical signals into optical signals to achieve visualization and quantitative analysis in parallel. The detection duration of this method is 1.5 h, the detection range is 10–1000 CFU mL^{-1}, and the detection limit reaches as low as 1.57 CFU mL^{-1}.

2. Materials and methods

2.1. Materials

5 mg mL^{-1} 500 nm streptavidin modified magnetic beads were purchased from Beijing Zhong Ke Lei Ming Dao Jin Technology Co. (Beijing, China). All DNA molecules used in this study came from Ruibio Biotech (Beijing, China). The details of the DNA sequences used in this study are listed in Table S1. *E. coli* O157:H7 (ATCC 43889) was obtained from American Type Culture Collection. T4 DNA ligase (400,000 U mL^{-1}), Phi29 DNA polymerase (10,000 U mL^{-1}), Exonuclease III (*E. coli*, 100,000 U mL^{-1}) and the low range ssRNA ladder marker were purchased from New England Biolabs (Beijing, China). 10 mM dNTP mixture, 6× loading buffer and 20 bp DNA ladder were purchased from Takara Biomedical Technology (Beijing, China). Trans2k DNA ladder was purchased from TransGen Biotech (Beijing, China). Alkaline phosphatase (200 U) was purchased from Beyotime Biotechnology (Beijing, China). TransStart Green qPCR SuperMix and ethidium bromide (EB) were purchased from Tiangen Biotech (Beijing, China). Anhydrous copper sulfate ($CuSO_4$) was bought from FuChen Chemical Reagent Co., Ltd. (Tianjing, China). Sodium ascorbate ($C_6H_7O_6Na$) was bought from Aladdin Biochemical Technology Co., Ltd. (Shanghai, China), while 3-morpholine propanesulfonic acid (MOPs), sodium chloride (NaCl), sodium hydroxide (NaOH) and boric acid were purchased from Macklin Reagent (Beijing, China). Magnesium chloride hexahydrate ($MgCl_2{\cdot}H_2O$) was purchased from Xiya Reagent (Shandong, China), N-2-hydroxyethylpiperazine-N-2-ethane sulfonic acid (HEPES) was purchased from Biosharp (China). Trihydroxymethyl aminomethane (Tris), Agar and ethylenediaminetetraacetic acid (EDTA) were purchased from Biotopped (Beijing, China). Agarose was purchased from Beijing Wobisen Technology Co., Ltd. (Beijing, China). Tryptone and yeast extract were purchased from Oxoid (England). MRS medium powder was purchased from Beijing Land Bridge Technology Co., Ltd. (Beijing, China). All other reagents used in this study were of analytical grade.

2.2. Methods

2.2.1. Preparation of crude intracellular mixture

The desired strain was activated under the appropriate conditions, and then cultured to $OD_{600} = 1$. Subsequently, 1 mL of the culture was poured into a sterile EP tube and centrifuged at 4 °C, 11,000 g for 5 min. Thereafter, 200 μL 1× Reaction buffer (RB: 100 mM HEPES, 300 mM NaCl, 30 mM $MgCl_2$) was added into the sediment and then the mixture was placed on the ice to ultrasonic oscillate with the ultrasonic power of 150 w for 10 min to ensure complete lysis of cells. The treated mixture was centrifuged at 4 °C, 11,000 g for 5 min again. The separated supernatant was CIM. Store it at −20 °C before use.

2.2.2. Determination of the E. coli-DNAzyme cleavage activity

The ligation of DNAzyme was according to the previous assay (Ali et al., 2011). 5 μL DNAzyme solution was mixed with 20 μL CIM and 25 μL 2× running buffer for 1 h. Subsequently, the reaction was terminated with 5 μL 3 M NaOAc (pH 7.0) and 100 μL iced 100% ethanol. To purify DNA, the solution was cooled at −20 °C for 1 h, after which the complex was centrifuged at 4 °C for 20 min, 11,000 g, and discarded the supernatant. The sediment was subsequently dried for 10 min. After adding 20 μl gel loading buffer (GLB) to suspend the DNA, the mixture was heated at 95 °C for 5 min, then immediately placed on ice to maintain its denatured state. The mixture with denatured treatment was characterized by the denatured PAGE to analyse the cutting ability of the DNAzyme.

2.2.3. Preparation of the magnetic DNAzyme complexes

10 μL 1 μM support chain modified by 5′-biotin and 10 μL 1 mg mL^{-1} magnetic beads modified by streptavidin were incubated at room temperature for 30 min. Thereafter, the sediment was magnetically separated by the magnetic force frames and washed again with the washing buffer. 10 μL 1 μM DNAzyme solution was added into the sediment and mixed gently (following the synthesis method described in section 2.2.2, the final concentration of DNAzyme is 10 μM). After 30 min incubation at room temperature, magnetic separation of removing the supernatant, and washing with the magnetic-bead buffer, the magnetic DNAzyme complexes were obtained.

2.2.4. Ligation and circularization of padlock probe

In order to ensure the smooth initiation of the RCA reaction, the cyclization of the padlock probe was finished before RCA. A non-complementary tail (G5) was introduced in the RCA primer (PrimerT20-G5, see in Table S1), which facilitated the smooth combination of the remaining fragments of DNAzyme cleavage and the replacement of the connecting chain. First, 10 μL 1 μM padlock probe and 10 μL 1 μM Primer T20-G5 were fully mixed, whereafter 3 μL 10× T4 DNA ligase buffer and 6 μL ddH_2O were added to be mixed on the scroll oscillator. The ligation system was heated at 65 °C for 5 min, followed by 37 °C for 30 min, and then the addition of T4 DNA ligase to react at room temperature for 2 h. The final solution was heated before use for 10 min at 75 °C.

2.2.5. RCA reaction and florescent detection based on CuNCs

The magnetic DNAzyme complexes were mixed with 20 μL 2× RB and 20 μL CIM, gently oscillated and incubated at room temperature for 1 h. Then the magnetic DNAzyme complexes were magnetically separated and washed twice with the washing buffer. Thereafter, 30 μL of the padlock got in 2.2.5, 5 μL 10× Phi29 DNA polymerase buffer, 12 μL 10 mM dNTPs, 1 μL BSA, and 2 μL Phi29 DNA polymerase were added to the separated sediment with gently mixing by a pipetting gun and cultured overnight in a shaker at 32 °C.

After that, the RCA product was mixed with 40 μL 10 mM sodium ascorbate solution, 20 μL 1 mM $CuSO_4$ solution, and 90 μL 10 mM MOPs buffer. The fluorescence intensity was measured under 340 nm excitation and 622 nm emission by the fluorescence spectrophotometer.

2.2.6. Detection of E. coli O157:H7 in real sample

The practicability of the biosensor was evaluated with *E. coli* O157:H7 spiked into drinking water (Nongfu Spring bottled water) and apple juice (Huiyuan). Overnight activated *E. coli* O157:H7 cultures were added to 5 mL of drinking water and 30% apple juice (about pH 7.0), and then cultured at 37 °C for 4 h, until the concentration of *E. coli* was about 8.7×10^5 CFU mL^{-1}. Then 1 mL of the sample was placed on the ice to ultrasonic oscillate with the ultrasonic power of 150 w for 10 min. After that, 20 μL of mixture was ready for the practicability test. Experiment with reaction buffer (RB) as an experimental control.

3. Results and discussion

3.1. Design idea of magnetic DNAzyme sensor

The *E. coli*-specific DNAzyme firstly hybridizes with the support chain modified by biotin through the complementary pairing (Scheme 1), while the magnetic beads modified with streptavidin are added for incubation to obtain the magnetic DNAzyme complexes which then mix with the crude intracellular mixture (CIM) of *E. coli* and perform the cleavage reaction. After the magnetic separation, the magnetic DNAzyme complexes containing the remaining segments can hybridize with the added padlock probes and initiate the RCA reaction. The obtained RCA products containing many poly-T sequences are taken as templates

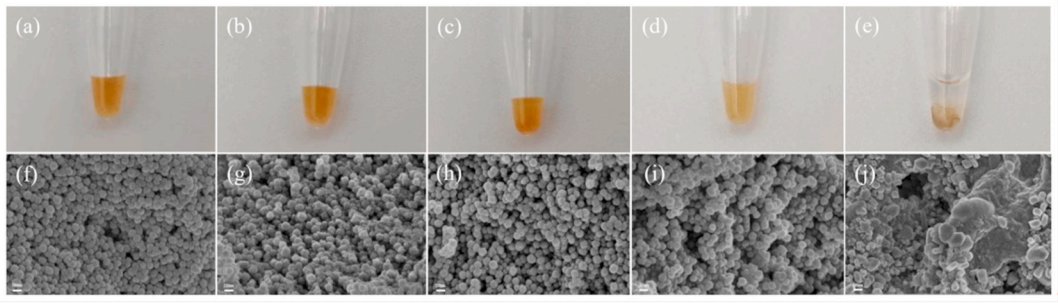

Fig. 1. Characterization of the magnetic DNAzyme complexes prepared as the procedures in 2.2.3. by naked-eye observation (upper row) and SEM (lower row, scale bars = 200 nm). a and f: Magnetic beads; b and g: Di-complexes of magnetic beads and support chain; c and h: Tri-complexes of magnetic beads, support chain and DNAzyme; d and i: Combinations of tri-complexes and CIM; e and j: RCA products (n = 6, P*<0.05).

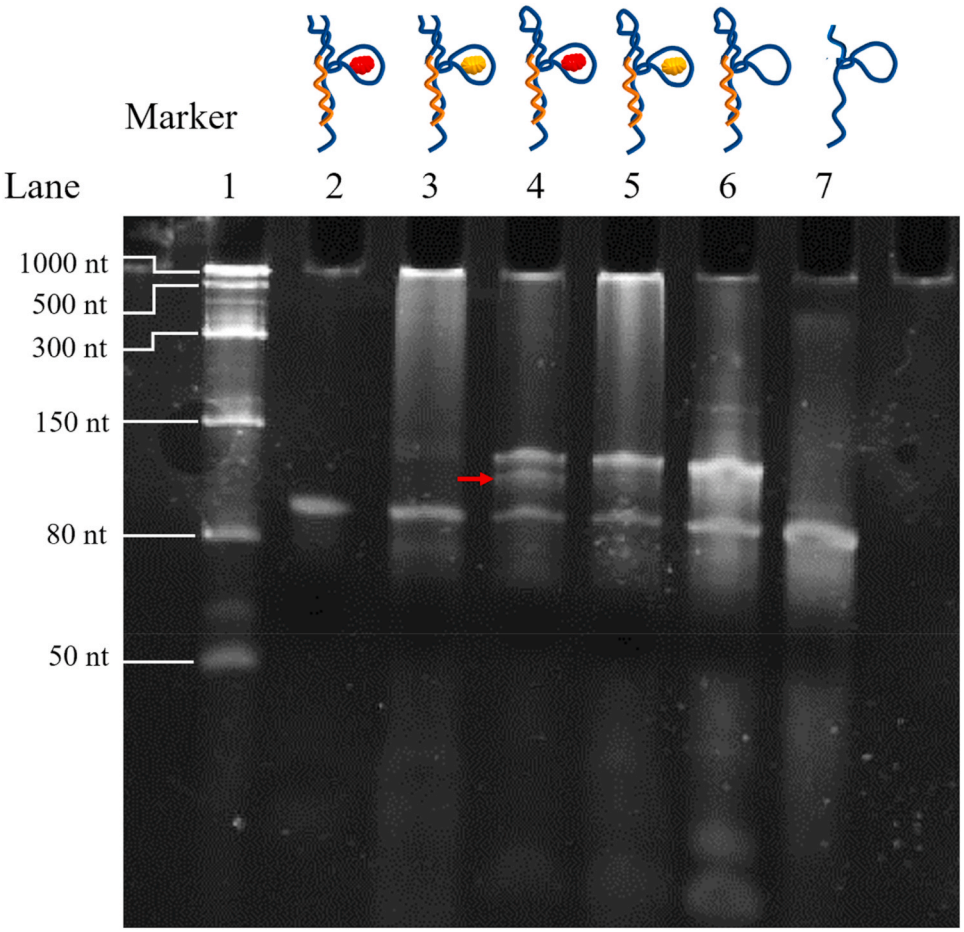

Fig. 2. Characterization of EC1-FS1 cleavage products with different optimization conditions processed as the procedures in 2.2.2. by 10% dPAGE. Lane 1: low-range ssRNA ladder marker (1000 nt, 500 nt, 300 nt, 150 nt, 80 nt, 50 nt from top to bottom, respectively); Lane 2: CIM + EC1+FS1; Lane 3: CEM + EC1+FS1; Lane 4: CIM + DNAzyme; Lane 5: CEM + DNAzyme; Lane 6: DNAzyme; Lane 7: EC1. The band pointed by the red arrow represented the cleavage products. (For interpretation of the references to colour in this figure legend, the reader is referred to the Web version of this article.)

to form CuNCs in the presence of copper sulfate and sodium ascorbate. CuNCs emit red light under ultraviolet light and their fluorescence intensity are easily measured to achieve the quantitative detection of *E. coli* O157:H7. (Sequences of oligonucleotides as presented in Table S1).

3.2. Morphology characterization of magnetic beads

The morphological characterization of magnetic beads as the carriers at different periods was carried out by naked-eye observation and SEM (Fig. 2), whose observation results were evaluated by integrating with the statistical analysis of the particle size (Table S2). It is indicated that the size of bare magnetic beads is around 200 nm, almost the same as that provided from the company (Fig. 1a and f). After combining with the support chain, the particle size of the magnetic complexes increased to 221 ± 15.41 nm (Fig. 1 b and g). The addition of the DNAzyme resulted in the particle size of the magnetic complexes further increased to 236 ± 10 nm (Fig. 1 c and h) which was 34 nm larger than that of the bare magnetic beads, while it fell to approximately 215 ± 6.9 nm after adding CIM (Fig. 1 d and i). These results confirmed the feasibility of this strategy that the closer connection between magnetic beads is based on a series of modifications and their different degrees of affinity. The relatively dispersed bare magnetic beads transform gradually into polymers modified with support chain which further ligated with DNAzyme, and they are finally covered by DNA amplification product and CuNCs after RCA reaction. It is interesting that the final polymer can be driven by

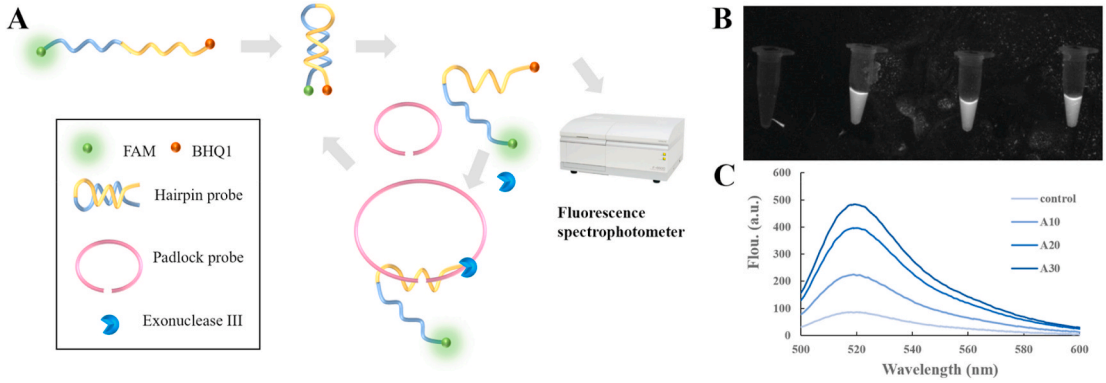

Fig. 3. The efficiency study of padlock circularization as the procedures in 2.2.4. (A) The experimental schematic diagram; (B) The luminescence of the fluorescent tag FAM under UV light. (the left-most one as control that contains only a fluorescent probe but without fluorescence due to the absence of a padlock); (C) The fluorescence intensity of Hairpin probe combined with different length Padlock probe (A10, A20, A30).

magnet. And it may be a simple model of magnetic machine. (Fig. 1 e and j, Movie S1).

3.3. Cleavage ability of DNAzyme

The self-cutting efficiency of the RNA site-cutting DNAzyme in the presence of the CIM was verified to be 47.1% (Fig. S2), which was approximately 1.17 times higher than crude extracellular mixture (CEM). The result is same as the previous report (Fig. 2 and 45%, Aguirre et al., 2013). In this characterization by PAGE, we also designed a trans-acting system by splitting the DNAzyme (EC1-FS1) into two parts (adaptor EC1 and substrate FS1) to omit the ligation time, which means that the EC1 and the FS1 were directly dispersed in the reaction system. However, the cleavage reaction in the trans-acting system only cut FS1 (28 nt) into two 14 nt fragments which was too short to be clearly shown in the PAGE results. Therefore, in the following experiment, we adopted the whole DNAzyme with CIM added.

3.4. Optimization of magnetic DNAzyme complexes

In order to get higher detection efficiency, we have optimized the concentration and co-incubation time of the support chain and DNAzyme. The 3′ end of the support chain was modified with a fluorescent tag FAM to determine the optimal concentration and reaction time of the connection between the support chain and the magnetic beads. The fluorescent group emitted green fluorescence under the wavelength of 522 nm excited by blue light with 494 nm wavelength, and its fluorescence intensity was detected by fluorescence spectrophotometer. The initial fluorescence intensity (namely the fluorescence intensity of combination at 0 min) was defined as I_0, and the fluorescence intensity measured during the reaction was set as I. Formula 1 was used to obtain the connection efficiency (a) between the support chain and the magnetic bead:

$$a = [(I_0–I)/I_0] \times 100\% \quad (1)$$

Numerous experiments and data demonstrate that the concentration of the support chain is related to the fluorescence intensity, but is not proportional to the connection efficiency when the concentration of the support chain is less than 0.01 μM and greater than 1 μM (Table S3). This may be due to the higher concentration of the support chain causing greater spatial resistance and the fact that the binding sites on the beads are already oversaturated. Besides, the support chains with high concentrations had high synthesis cost and low utilization rate, and thus, concentrations of 10 μM were not recommended. However, the support chain with extremely-low concentration (0.001 μM) may result in low fluorescence intensity and obvious fluorescence instability. Thus, it was also not recommended to use extremely-low concentrations which may cause great errors. Moreover, when the reaction time was 20–40 min, the connection efficiency between the support chain and magnetic beads was high. Among them, the maximum connection efficiency was found at the support chain with a concentration of 1 μM, while the fluorescence intensity at a concentration of 0.01 μM increased first and then tend to balance, which was more consistent with common sense. Therefore, the optimized range of concentration was reduced to 1–0.01 μM, and that of time was reduced to 20–40 min for further detection (Table S3). After further narrowing the concentration range (Table S4), we found that when the concentration of the support chain was 1 μM, the connection efficiency gradually stabilized with time, so we chose 1 μM for subsequent experiments. And the incubation time is 30 min.

The magnetic bead-support chain complexes were obtained after repeatedly removing the non-specific binding of the support chain on the surface of magnetic beads by the magnetic separation, which prepared for the following DNAzyme connection. After that, the support chain-magnetic bead complexes performed the coupling reaction with DNAzyme and the connection efficiency of it was determined by qPCR (forward and reverse primers as shown in Table S1). Each sample was diluted 10^3 times in accordance with Table S5 to join the corresponding reagents of qPCR and to finally obtain clear liquid from them. The initial concentration of DNAzyme and the concentration of it in the clear solution were defined as C_0 and C, respectively. Formula 2 was used to calculate the connection efficiency (b) of DNAzyme:

$$b = [(C_0–C)/C] \times 100\% \quad (2)$$

The standard qPCR curve was plotted with a concentration gradient of DNAzyme. The Cq value obtained from the reaction was substituted into the standard curve formula to calculate the concentration C. As shown in Fig. S4 and Table S6, the results revealed that 0.1 μM and 1 μM are optimum concentrations of DNAzyme. In order to save the reagent, 0.1 μM DNAzyme was selected for the following experiments.

3.5. The efficiency study of padlock circularization

In order to make the RCA proceed smoothly, the efficiency of the padlock circularization with 24 nt-44 nt poly-adenine (A) single-stranded DNA (ssDNA) in the RCA reaction was investigated. The principle of the optimization experiment is shown in Fig. 3A.

In order to verify the occurrence of circularization, we designed a fluorescent probe with obvious hairpin structure of which 5′ end was modified with the fluorescent groups FAM and 3′ end was modified with the quenching group BHQ1 (Table S1). When the hairpin structure formed, the fluorescence was quenched. On the contrast, when it opened, the fluorescence was restored. And the method is as following part: 10 μL 10 μM padlock probe was heated for 10 min and then immediately refrigerated at 4 °C for denaturation. After 5 min, it was

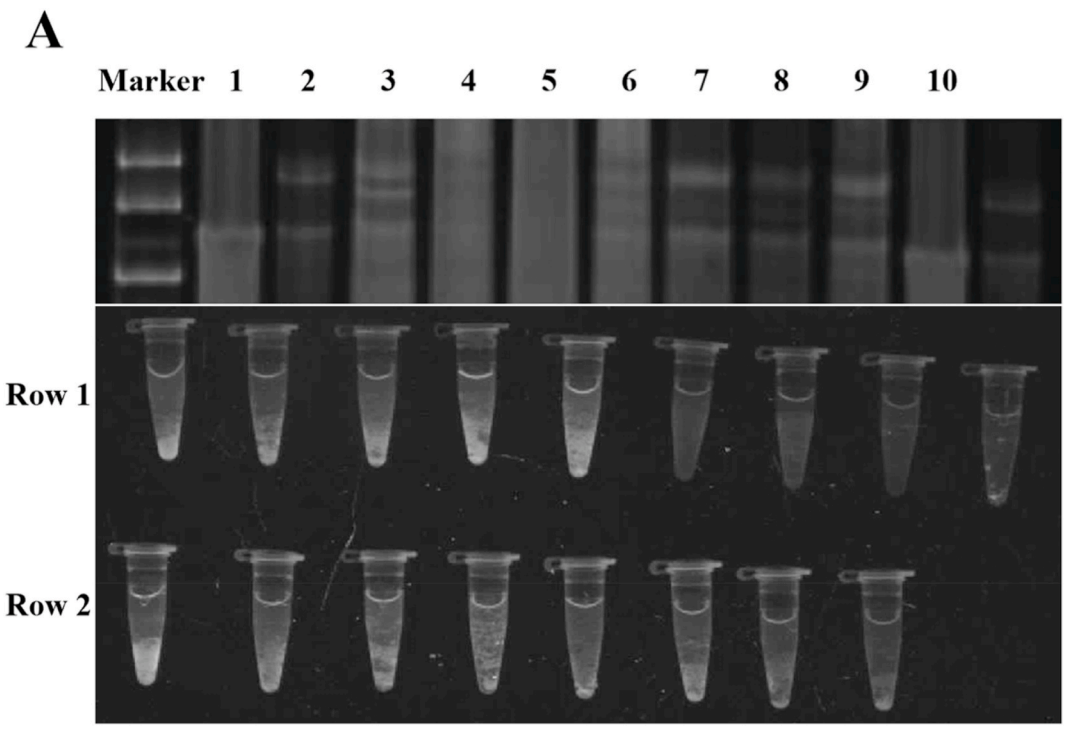

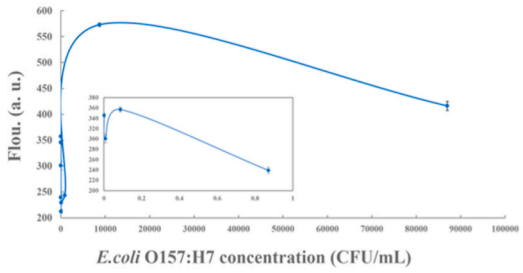

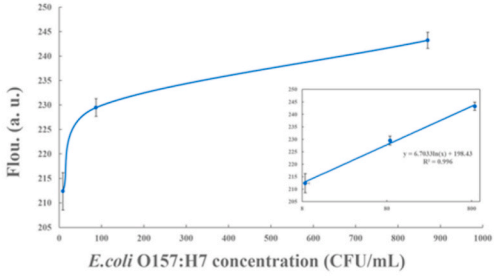

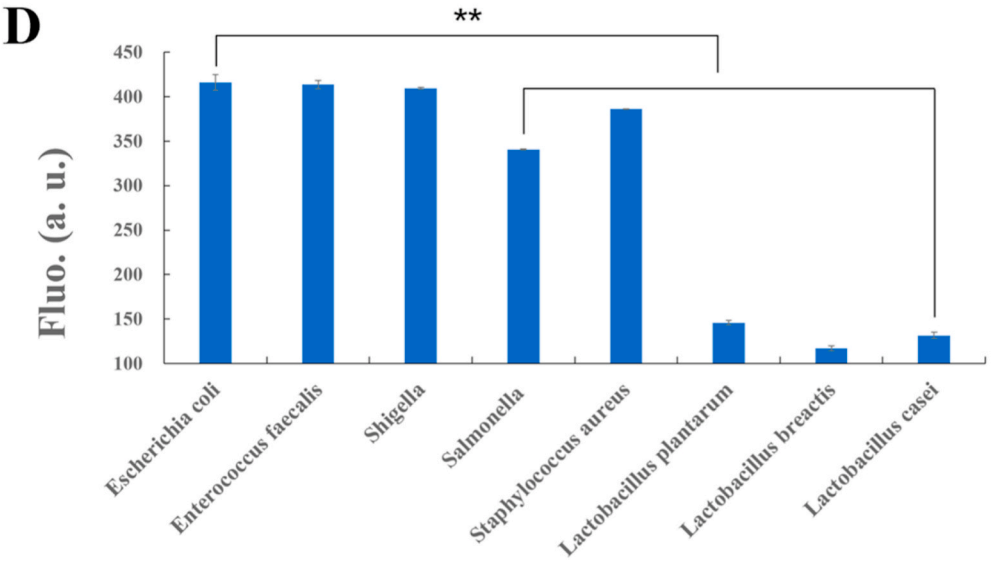

(caption on next page)

Fig. 4. Results of the specificity and sensitivity tests as the procedures in 3.6. (A) Image of the denatured polyacrylamide gel electrophoresis (dPAGE) (top inset). Lane 1–10 represent DNA molecular marker, EC1, RFD-EC1, *Escherichia coli*, *Staphylococcus aureus*, *Shigella*, *Salmonella*, *Lactobacillus casei*, *Lactobacillus breactis, Lactobacillus plantarum,* and CIM-magnetic DNAzyme complexes, respectively; Image of ultraviolet irradiation after forming CuNCs (Bottom inset). The samples in row 1 from left to right represent *Escherichia coli*, *Enterococcus faecalis*, *Salmonella*, *Staphylococcus aureus*, *Shigella*, *Lactobacillus plantarum*, *Lactobacillus breactis*, *Lactobacillus casei,* and CIM-magnetic DNAzyme complexes, respectively. The results of the row 2 from left to right represents samples with the 10^{-1}-10^{-8} diluted multiples of *E. coli,* and CIM-magnetic DNAzyme complexes, respectively; (B) Results of fluorescence intensity at 622 nm at concentrations of *E. coli* O157:H7 ranging from 8.7×10^{-4} to 8.7×10^{4} CFU mL^{-1}. The inset shows the corresponding fluorescence intensity at 622 nm at low concentration of it ranging from 8.7×10^{-4} to 8.7×10^{-1} CFU mL^{-1}; (C) Linear correlation between fluorescence intensity at 622 nm and concentrations of *E. coli* O157:H7 ranging from 8.7 to 8.7×10^{2} CFU mL^{-1}. The inset shows the standard curve; (D) the specificity test.

taken out and mixed thoroughly with a 10 μL 10 μM hairpin probe for 1–2 min. Thereafter, 7 μL Exonuclease III buffer, 3 μL Exonuclease III and 30 μL water were added immediately. The PCR tube was wrapped in tinfoil throughout. The fluorescence intensity was measured under 492 nm excitation and 518 nm emission by a fluorescence spectrophotometer (Cary Eclipse, Agilent Technologies, USA).

The results showed that the padlock probe with poly A30 possessed with the highest circularization efficiency (%), while it with poly A10 reached the minimum circularization efficiency (%) (Fig. 3B and C). The reason is supposed that with fixing the length of complementary part of the hairpin probe, the shorter the length of the padlock probe, the more difficult the connection of two ends of the hairpin probe, which means the greater the required tension of connecting two ends. In the padlock probe with the poly A10, the length of the complementary section is 14 nt, and only 10 nt in length is left in the middle for the circularization. Therefore, compared to the poly A30 remaining 20 nt for the circularization, the circularization efficiency of the poly A10 was relatively low. However, the whole length of the padlock probe with poly A30 was 44 nt which was long enough to have an influence on the circularization efficiency (Sasaki et al., 2017, 2020; Song et al., 2019a,b, 2020). Due to shorter in whole length with higher circularization efficiency, the padlock probe with poly A20 was selected for the RCA reaction, and the reaction time of RCA was 0.5 h under optimization (Fig. S4).

3.6. Sensitivity test and specificity test

We made different preparations before the sensitivity and specificity experiments. On the one hand, the extracted CIM of *E. coli* O157:H7 was subjected to gradient dilution of 10^{0} to 10^{-8} for the sensitivity test. On the other hand, we obtained various CIM from three common probiotics, including *Lactobacillus casei*, *Lactobacillus breactis*, and *Lactobacillus plantarum*, and four common pathogens, including *Salmonella*, *Shigella*, *Enterococcus faecalis*, and *Staphylococcus aureus* for the specificity test, the CIM from whom haven't been used in a specificity test ever (Ali et al., 2011; Aguirre et al., 2013; Liu et al., 2016, 2017).

Before the sensitivity test, we have correlated the concentration of CIM with the concentration of bacteria. We use the flat colony counting method to get Colony Forming Unit (CFU) of 1 mL E. *coli* O157:H7 ($OD_{600} = 1$), and the result is 8.7×10^{5} CFU mL^{-1}. In addition, 20 μL CIM was added into the reaction system, so the final concentration of *E. coli* in tube was 8.7×10^{-4}-8.7×10^{4} CFU mL^{-1} respectively. The experimental result shows a certain linear relationship between 8.7 and 8.7×10^{2} CFU mL^{-1} (Fig. 4C). Therefore, it was preliminarily estimated that the detection range of this strategy was 10–10^{3} CFU mL^{-1}. Then we obtained the detection limit of 1.57 CFU mL^{-1} by using formula (3s/slope, s = standard deviation of blank group, slope = the slope of the linear equation, Hui et al., 2018).

And for the specificity test, the significant specificity of *E. coli* and the long-term specificity of DNAzyme were respectively observed according to the final experimental results of the formed CuNCs in Fig. 4D and a comparison of 10% dPAGE results in Fig. 4A. However, there was no significant difference between the detection results of *E. coli* O157:H7, *Enterococcus faecalis* and *Shigella*. We analysed the possible reasons were as follows: (1) These three strains may have a closer homology or belong to a similar protein induced by the same ecosystem (Trieu-Cuot et al., 1988; Lan et al., 2004). (2) More importantly, it is uncertain which target protein is involved in the fragmentation of DNAzyme (Ali et al., 2011; Aguirre et al., 2013; Li, 2011). Based the above reasons, if all these three bacteria contain the same target protein, it is likely to obtain the present results. Therefore, our next step is to find the target protein hidden in CIM. These insignificant differences will lay the foundation for our future research. In brief, this sensor was not sensitive to human intestinal probiotic lactobacillus, slightly sensitive to pathogenic bacteria, and particularly sensitive to the target bacteria *E. coli*.

3.7. Practicability test of the sensor

Finally, we tested the practicability of the sensor in drinking water and apple juice contaminated with *E. coli* O157:H7 (Fig. S5). The results showed that the sensor could detect *E. coli* in both pure drinking water and apple juice. And compared with the control group, this sensor shows better practicability.

4. Conclusion

In conclusion, we designed a thermostatic, and ultrasensitive magnetic DNAzyme-CuNCs fluorescent biosensor for the detection of *E. coli* O157: H7 in complex environment. With incorporation of several FNAs and magnetic beads into the RCA reaction, this biosensor can successfully realize triple amplification and dual output of signal. Especially, it exhibited high-sensitivity response to other pathogenic bacteria of the intestinal bacteria genus. Compared with similar type of biosensors reported in 2016–2020 (Table S10), the magnetic DNAzyme-CuNCs fluorescent biosensor with manifold superiorities displays strong potential for detecting broad-spectrum pathogens. The sensor also has the potential for rapid detection, namely the ability to directly extract samples for detection. Although there are some deficiencies, such as low specificity for homologous bacteria, we may be able to use it to develop more sensitive broad-spectrum sensors. In addition, we are analyzing the target protein in CIM to explore its interaction with DNAzyme, thereby changing the mode of bacteria-DNAzyme screening in vitro. And ultimately, the specificity and sensitivity of in vitro screening and detection will be improved.

CRediT authorship contribution statement

Ziqi Zhou: Conceptualization, Methodology, Validation, Formal analysis, Data curation, Writing - original draft. **Yangzi Zhang:** Methodology, Validation, Formal analysis, Writing - review & editing. **Mingzhang Guo:** Investigation, Data curation, Resources. **Kunlun Huang:** Conceptualization, Methodology, Supervision. **Wentao Xu:** Conceptualization, Supervision, Project administration, Funding acquisition.

Declaration of competing interest

The authors declare that they have no known competing financial interests or personal relationships that could have appeared to influence the work reported in this paper.

Acknowledgements

This work is financially supported by the National Natural Science

Foundation Project of China (31871875) and the Key R&D Project of Yunnan Province: Social Development Field (2018BC006).

Appendix A. Supplementary data

Supplementary data to this article can be found online at https://doi.org/10.1016/j.bios.2020.112475.

References

Aguirre, S.D., Ali, M.M., Salena, B.J., Li, Y., 2013. Biomol. 3, 563–577.
Ali, M.M., Aguirre, S.D., Lazim, H., Li, Y., 2011. Angew. Chem. Int. Edit. 50, 3751–3754.
Ali, M.M., Aguirre, S.D., Mok, W.W., Li, Y., 2012. Methods Mol. Biol. 848, 395–418.
Ali, M.M., Brown, C.L., Jahanshahi-Anbuhi, S., Kannan, B., Li, Y., Filipe, C.D.M., Brennan, J.D., 2017. Sci. Rep. 7, 12335.
Bedasa, S., Shiferaw, D., Abraha, A., Moges, T., 2018. Int. J. Food. Contam. 5, 2.
Cho, E.J., Yang, L., Levy, M., Ellington, A.D., 2005. J. Am. Chem. Soc. 127, 2022–2023.
Chen, Y., Cheng, N., Xu, Y., Huang, K., Luo, Y., Xu, W., 2016. Biosens. Bioelectron. 81, 317–323.
Cho, I.H., Bhandari, P., Patel, P., Irudayaraj, J., 2015. Biosens. Bioelectron. 64, 171–176.
Cooper, K.K., Mandrell, R.E., Louie, J.W., Korlach, J., Clark, T.A., Parker, C.T., Huynh, S., Chain, P.S., Ahmed, S.A., Carter, M.Q., 2014. BMC Genom. 15, 1–17.
Flynn-Charlebois, A., Wang, Y., Prior, T., Rashid, I., Hoadley, K., Coppins, R., Wolf, A., Silverman, S., 2003. J. Am. Chem. Soc. 125, 2444–2454.
Gong, L., Zhao, Z., Lv, Y.F., Huan, S.Y., Fu, T., Zhang, X.B., Guo, L.S., Ru, Q.Y., 2015. Chem. Commun. 51, 979–995.
Guo, M., Wang, J., Du, R., Liu, Y., Chi, J., He, X., Huang, K., Luo, Y., Xu, W., 2019. Biosens. Bioelectron. 150, 111899.
Hui, C.Y., Liu, M., Li, Y., Brennan, J.B., 2018. Angew. Chem. Int. Edit. 57, 4549–4553.
Lan, R., Alles, M.C., Donohoe, K., Martinez, M.B., Reeves, P.R., 2004. Infect. Immun. 72 (9), 5080–5088, 2004.
Li, Y.F., 2011. Future Microbiol. 6, 973–976.
Liu, J., 2014. TrAC Trends Anal. Chem. (Reference Ed.) 58, 99–111.
Liu, M., Zhang, Q., Chang, D., Gu, J., Brennan, J.D., Li, Y., 2017. Angew. Chem. Int. Edit. 56, 6142–6146.
Liu, M., Zhang, Q., Li, Z., Gu, J., Brennan, J.D., Li, Y., 2016. Nat. Commun. 7, 12074.
Lv, S., Li, Y., Zhang, K., Lin, Z., Tang, D., 2017a. ACS Appl. Mater. Interfaces 9, 38336–38343.
Lv, S., Zhang, K., Lin, Z., Tang, D., 2017b. Biosens. Bioelectron. 96, 317–323.
Ma, F., Zhang, C.X., 2019. Chin. J. Anal. Chem. 37, 107.
McConnell, E.M., Morrison, D., Alejandra, R.R.M., Salena, B.J., Li, Y., 2020. TrAC Trends Anal. Chem. (Reference Ed.) 124, 1–12.
Qing, T., He, X., He, D., Ye, X., Shangguan, J., Liu, J., Yuan, B., Wang, K., 2017. Biosens. Bioelectron. 94, 456–463.
Qing, Z., He, X., He, D., Wang, K., Yang, X., 2013. Angew. Chem. Int. Edit. 52, 9901–9904.
Rothenbroker, M., Zakaria, S., Morrison, D., Li, Y.F., 2019. DNAzymes: Synthetic enzymes made of DNA: Biocatalysis. In: Husiain, Q., Ullah, M.F. (Eds.), Biocatalysis: Enzymatic Basics and Applications. Springer, Boston, pp. 1–16.
Saeedi, P., Yazdanparast, M., Behzadi, E., Salmanian, A.H., Nazarian, S., Mousavi, S.L., Amani, J., 2017. Microb. Pathog. 103, 186–195.
Sasaki, N., Gunji, Y., Kase, C., Sato, K., 2017. Anal. Biochem. 519, 15–18.
Sasaki, N., Kase, C., Chou, M., Nakazato, G., Sato, K., 2020. Anal. Biochem. 593, 113596.
Satyavolu, N., Loh, K., Tan, L., Lu, Y., 2019. Small 15, 1900975.
Sluijter, J., Pasterkamp, G., Kleijn, D., 2006. Quantitative real-time PCR. In: Pasterkamp, G., Kleijn, D. (Eds.), Cardiovascular Research. Springer, Boston, pp. 75–83.
Song, H., Zhang, Y., Cheng, P., Chen, X., Luo, Y., Xu, W., 2019a. Chem. Commun. 55, 5375–5378.
Song, H., Zhang, Y., Wang, S., Huang, K., Luo, Y., Zhang, W., Xu, W., 2020. Sens. Actuator B Chem. 306, 127554.
Song, S., Wang, X., Xu, K., Xie, G., Yang, X., 2019b. J. Agric. Food Chem. 67, 1244–1253.
Tian, J., Chu, H., Zhang, Y., Li, K., Tian, H., Zhang, X., Xu, W., 2019. ACS Appl. Mater. Interfaces 11, 46504–46514.
Tram, K., Kanda, P., Salena, B., Huan, S., Li, Y., 2014. Angew. Chem. Int. Edit. 53, 12799–12802.
Trieu-Cuot, P., Carlier, C., Courvalin, P., 1988. J. Bacteriol. 170, 4388–4391.
Vaish, N.K., Jadhav, K., Kossen, V.R., Pasko, C., Seiwert, S.D., 2003. RNA 9, 1058–1072.
Wang, S., Xie, J., Jiang, M., Chang, K., Chen, R., Ma, L., Zhu, J., Guo, Q., Sun, H., Hu, J., 2016. Sens. 16, 1856.
Xia, J., Wang, W., Hai, X., E, S., Shu, Y., Wang, J., 2019. Chin. Chem. Lett. 30, 421–424.
Xiao, X., Zhu, L., He, W., Luo, Y., Xu, W., 2019. TrAC Trends Anal. Chem. 118, 138–157.
Xu, M., Wang, R., Li, Y., 2016. Talanta 148, 200–208.
Xu, W., He, W., Du, Z., Zhu, L., Huang, K., Lu, Y., Luo, Y., 2019. Angew. Chem. Int. Edit. https://doi.org/10.1002/anie.201909927.
Yang, D., Guo, Z., Tang, Y., Miao, P., 2017. ACS Appl. Nano Mater. 1, 168–174.
Yousefi, H., Ali, M.M., Su, H.M., Filipe, C.D.M., Didar, T.F., 2018. ACS Nano 12, 3287–3294.
Yu, F., Li, Y., Li, M., Tang, L., He, J.J., 2017. Biosens. Bioelectron. 89, 880–885.
Zhang, K., Lv, S., Lin, Z., Tang, D., 2017. Biosens. Bioelectron. 95, 34–40.
Zhou, Q., Lin, Y., Lin, Y., Wei, Q., Chen, G., Tang, D., 2016. Biosens. Bioelectron. 78, 236–243.
Zhu, L., Xu, Y., Cheng, N., Xie, P., Shao, X., Huang, K., Luo, Y., Xu, W., 2017. Sens. Actuator B Chem. 242, 880–888.